ACS Energy LETTERS

http://pubs.acs.org/journal/aelccp

4-T CdTe/Perovskite Thin Film Tandem Solar Cells with Efficiency >24%

Ananta Paul,[†] Abhijit Singha,[†] Kashimul Hossain,[†] Saurabh Gupta, Manas Misra, Sudhanshu Mallick, Amit H. Munshi, and Dinesh Kabra*

Cite This: *ACS Energy Lett.* 2024, 9, 3019−3026

Read Online

ACCESS | Metrics & More | Article Recommendations | Supporting Information

ABSTRACT: **An integration of perovskite and cadmium telluride (CdTe) solar cells in a tandem configuration has the potential to yield efficient thin-film tandem solar cells. Owing to the promise of higher efficiency at low cost, the presented study aims to explore the potential for combining this commercially established CdTe photovoltaics (PV) with next-generation perovskite PV. Here, we developed four-terminal (4-T) CdTe/perovskite tandem solar cells, starting with 18.3% efficient near-infrared-transparent perovskite solar cells (NIR-TPSCs) with an average transmission (T_{avg}) of 24.76% in the 300−900 nm wavelength range. These were then integrated with 19.56% efficient opaque CdTe solar cells, achieving 23.42% efficiency in a 4-T tandem configuration. Additionally, using a refractive index matching liquid increases the overall power conversion efficiency (PCE) to 24.2%. This pioneering achievement marks the first instance of a 4-T CdTe/perovskite thin-film tandem solar cell exceeding a PCE of 24.2%, a significant 123.72% increase in overall PCE.**

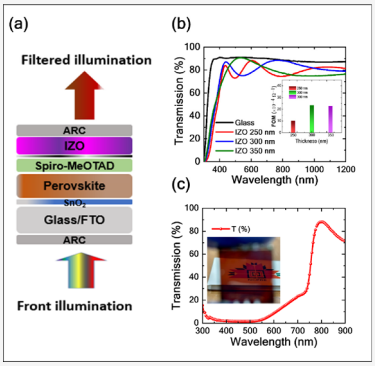

The terrestrial photovoltaic market is currently dominated by monocrystalline silicon solar cells, providing electricity generation at a cost as low as $1−$1.5 per watt, with a lifespan of up to 40 years.[1] However, the industry faces a formidable challenge in pushing the boundaries of cost-effectiveness for power generation, primarily due to the higher material consumption and saturation of power conversion efficiency (PCE). In this context, cadmium telluride (CdTe) solar cells emerged as a viable solution to address these challenges. CdTe is known as the most efficient and commercially proven technology following monocrystalline silicon solar cells. It possesses an optimum bandgap with high absorption coefficient, leading to an efficient and cost-effective semiconductor for PV applications. The CdTe photoabsorber can absorb the majority of the AM1.5G solar spectrum with a mere 2 μm thick film, which directly contributes to relatively lower production costs. Additionally, CdTe solar cells are free from wafer fabrication complexities, as their thin films can be grown onto commercially available and inexpensive glass substrates with relative ease and excellent repeatability. Notably, CdTe solar cells have demonstrated the highest PCE of up to 22.3% on their near-ideal bandgap, further solidifying their position as a promising alternative in solar energy harvesting devices.[2] While CdTe presents a promising avenue for achieving cost-effective electricity generation, its practical application is constrained due to a relatively lower PCE. The challenges associated with the lower PCE of CdTe solar cells can be addressed by adapting multijunction or tandem cell configurations. A critical prerequisite for efficient tandem solar cells is incorporating suitable wide bandgap-based transparent solar cells.[3] Third-generation photoabsorbers, particularly perovskites, have demonstrated superiority by exhibiting excellent photovoltaic performance due to higher light absorption coefficient.[4−6] The ease of bandgap tuning further adds to the advantageous characteristics of perovskite materials.[7,8]

Perovskite has been aggressively explored in the fabrication of tandem solar cells with the most commercial monocrystalline Si bottom cells, and within a very short time span, the Si/perovskite monolithic tandem solar cells beat the S-Q limits of single junction solar cells. Notably, it is not only monocrystalline Si, the perovskite is also explored on thin-film tandem solar cell fabrications such as CIGS/perovskite, CIS/perovskite, and organic/perovskite tandem solar cells.[9−16] Furthermore, it is found that the 4-T tandem configuration is technically superior to 2-T, as it is free from fabrication complexities and current matching requirements.[17−19] The 4-T configuration relies solely on optical coupling between the two subcells. Owing to the above mentioned superiority of the 4-T

Received: April 23, 2024
Revised: May 21, 2024
Accepted: May 24, 2024

https://doi.org/10.1021/acsenergylett.4c01118
ACS Energy Lett. 2024, 9, 3019−3026

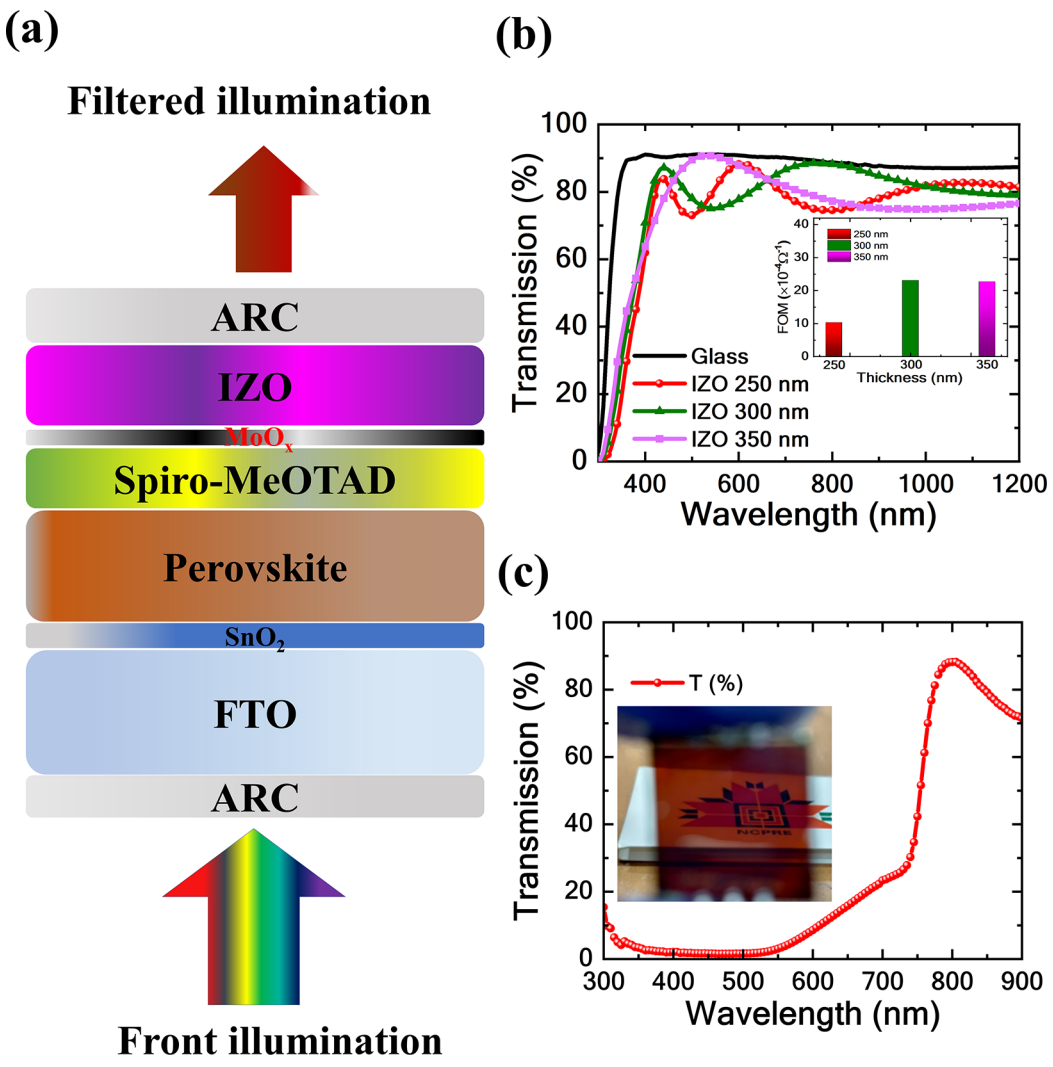

Figure 1. (a) Schematic representation of the NIR-TPSCs architecture. (b) Transmission and FOM (inset) of TCE with varying thicknesses from 250 to 350 nm. (c) Transmission spectrum of NIR-TPSCs. Inset shows a photographic image of the NIR-TPSCs.

tandem solar cell architecture, here we have focused only on 4-T tandem solar cells. Kim et al. reported the highest PCE of 25.9% over an active area of 0.45 cm^2 for a four terminal (4-T) perovskite/CIGS thin-film tandem solar cell, through the incorporation of bimolecular additives in the wide-bandgap perovskite solar cell.[20] Wang et al. reported the highly efficient all perovskite 4-T tandem solar cell with PCE ~ 26.24%.[21] Also, Ling Liu et al. demonstrated a perovskite/organic 4-T thin-film-based tandem solar cell with PCE of ~22%.[22] These results along with known bandgap tunability further confirm the superiority of perovskite photoabsorber for tandem solar cells. The dry fabrication process compatibility of both CdTe and perovskite solar cells is also another beneficial factor.[23,24]

The CdTe solar cell has the most potential among all established technologies to compete against a rapid increase in silicon solar cell efficiency at a significantly lower cost than commercial Si solar cells, as per recent reports.[25,26] Additionally, as a thin film photovoltaic technology, i.e., similar to the perovskite photovoltaics, the complexities associated with the commercial adeptness can be minimized. It also enables the development of a new tandem architecture, such as the development of tandem solar cells on a single glass substrate.[27] Therefore, the robustness of these thin-film tandem solar cells with the intrinsically lowest material consumption can proffer the development of the most efficient and cost-effective thin-film tandem photovoltaics. Despite promising thin-film tandem solar cells, only a limited number of reports are available, and to the best of our knowledge, not a single report is available on the experimental results of tandem CdTe/perovskite. There is only one theoretical simulation study of the theoretical viability of tandem CdTe/perovskite reported so far, where they proposed the viability of this technique with a maximum PCE of 20.6%.[28]

In this work, we have reported an experimental demonstration of 4-T CdTe/perovskite tandem solar cells for the first time, to our knowledge by mechanically stacking near-infrared (NIR) transparent wide bandgap (E_g ~ 1.63 eV) perovskite as top cells and low-bandgap CdTe (E_g ~ 1.39 eV) as bottom cells. We have fabricated 18.3% efficient NIR-transparent perovskite solar cells (NIR-TPSCs) depending on our unique optimization of an efficient sputtered top transparent electrode and buffer layer. With the integration of the 18.30% efficient NIR-TPSCs to 19.56% efficient CdTe solar cells in 4-T tandem configuration, we have achieved 24.2% of the highest PCE. Our fabricated device also possesses the remarkable stability of T_{80} for more than 3000 h at dark storage conditions

https://doi.org/10.1021/acsenergylett.4c01118
ACS Energy Lett. 2024, 9, 3019−3026

(N_2 glovebox). This work enables the first experimental observation of 4-T CdTe/perovskite tandem cells with more than 24% PCE. Eventually, this 4-T tandem cell observes a significant PCE boost of ~24%, i.e., 19.56% → 24.2%.

Figure 1a shows the device schematic of *n-i-p* architecture-based NIR-TPSCs. The device structure consists of MgF_2/glass/FTO/SnO_2/perovskite/spiro-MeOTAD/MoO_x/TCE/MgF_2. The incident solar radiation irradiates from the glass/FTO side, and the filtered rays are transmitted through the complete device stack. Eventually, the triple-cation perovskite absorber material with the chemical composition $Cs_{0.05}(MA_{0.17}FA_{0.83})_{0.95}Pb(I_{0.83}Br_{0.17})_3$ is used here to fabricate NIR-TPSCs. This perovskite absorber is well known and most widely studied perovskite due to its robustness under ambient conditions and lower fabrication complexity.[29,30] The transparency of NIR-TPSCs is another criterion that establishes the versatility of these solar cells for tandem applications. Figure 1b shows the transmission spectrum and Figure of Merit (FOM) of the TCE with varying thickness starting from 250 nm to 350 nm in steps of 50 nm. The detailed explanation of FOM is described in **Note 1** of SI. As the thickness increases, the transmission and the FOM also increase up to 300 nm, and after that, the average transmission (T_{avg}) and FOM decrease primarily because of the reflection of the TCE layer. An increased thickness of the TCE layer provides a better FOM; however, one needs to be careful about possible sputter damage while optimizing the TCE layer on top of such a device stack.[31] In the *n-i-p* structure, it is relatively forgiving due to the thicker layer of the spiro-MeOTAD HTL layer. Therefore, we have fixed the TCE layer thickness of 300 nm for further analysis. Figure 1c shows the transmission spectrum of the NIR-TPSCs at wavelengths 300−900 nm. The transmission spectrum sharply rises around ~750 nm and reaches its maximum transmission of 86.76%; after that, it varies periodically due to encountering interference effects. It shows T_{avg} ~ 75% in the 750−900 nm wavelength range. However, the average transmittance in NIR range (800−900 nm) ($T_{NIR,avg}$) of the NIR-TPSCs device is more than 78%. A marginal reduction in the transmission is also observed in the NIR region, which can be attribute to parasitic absorption loss of the TCE. The origin of the parasitic absorption in the NIR range is due to free carrier absorption. These could be reduced further by process optimization and varying the TCE layer thickness. An antireflection coating is also inserted on both sides of the device to further reduce the optical reflection losses.[32−34] Figure 1c (inset) shows the digital image of the actual device without a metal (Ag) busbar and with fingers of artificial light from the front side.

An adequate electron coupling is established as per the previous reports and the corresponding energy band diagram of the NIR-TPSCs devices (Figure S1).[35] The cross-sectional FESEM image depicts each individual layer of optimum thickness of the complete device, i.e., glass/FTO (400 nm)/SnO_2 (35 nm)/perovskite (460 nm)/Spiro-MeOTAD (180 nm)/MoO_x (8 nm)/TCE (300 nm)/ARC (MgF_2) (110 nm) (Figure S2). Figure 2a shows the (J−V) characteristics in both forward scan (FS) and reverse scan (RS) directions under 1-Sun illumination (at 25 °C, relative humidity ~ 40%) for the NIR-TPSCs. The champion device having active area (aa) = 0.175 cm^2 gives V_{OC} = 1.07 V, J_{SC} = 23.75 $mAcm^{-2}$, and FF = 72%, leading to a PCE of 18.3%. The large-area device having aa = 0.805 cm^2 gives V_{OC} = 1.04 V, J_{SC} = 23.24 $mAcm^{-2}$, and FF = 63.0%, leading to a PCE of 15.23%. We used Ag busbars

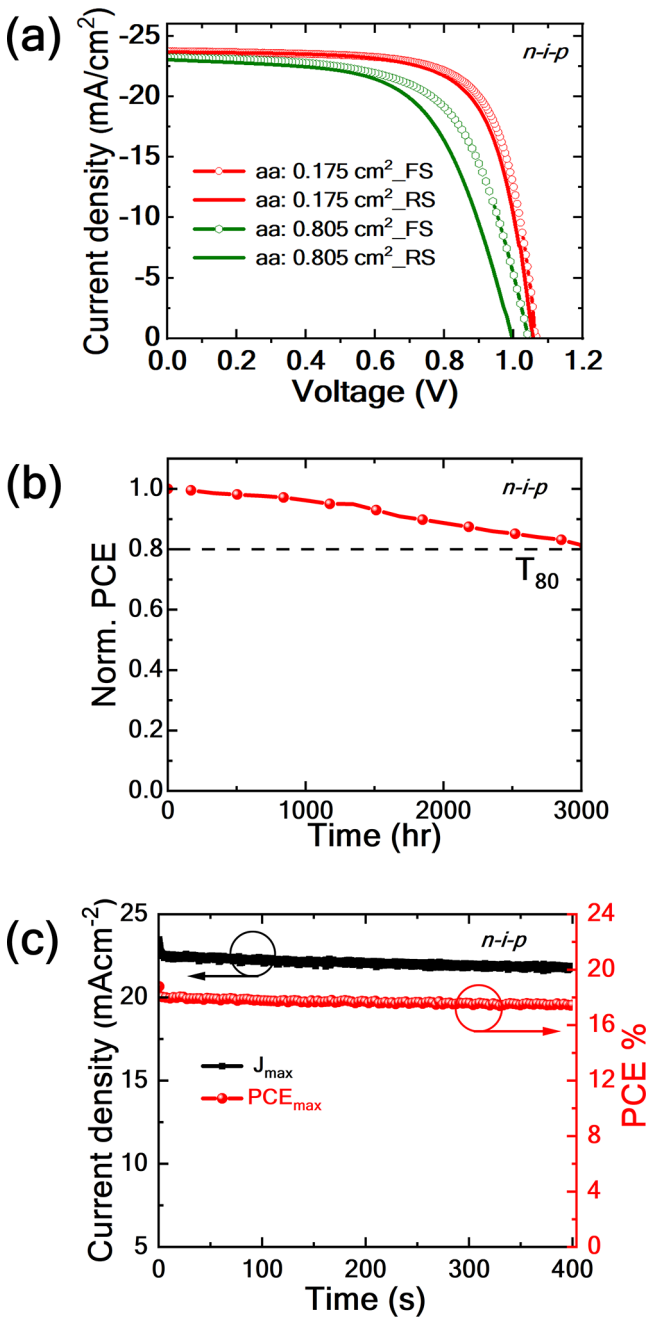

Figure 2. (a) Current−voltage (J−V) characteristics of the NIR-TPSCs. (b) Stability data of NIR-TPSCs at T_{80} >3000 h in dark condition in a N_2 glovebox. (c) Light induced photocurrent density and corresponding PCE at the MPPT of the NIR-TPSCs.

in the large-area devices to further reduce the effective sheet resistance of the TCE.[36,37] The actual dimensions of the metal busbars and fingers are 8 × 1 mm^2 and 4.5 × 0.3 mm^2 (Figure S3). The statistical findings of the NIR-TPSCs concerning their PCE are illustrated in Figure S4. Table 1 shows the J−V parameters of both small- and large-area based NIR-TPSCs. Additionally, a small amount of hysteresis and V_{OC} deficit is also observed in large-area PSCs devices, which can be due to the effect of higher series and lower shunt resistance (Table S1).[38,39]

Figure 2b shows the unencapsulated devices' operational stability in an N_2 glovebox (ISOS-D). The devices retain more than 80% of their initial PCE, even after being stored for 3000

https://doi.org/10.1021/acsenergylett.4c01118
ACS Energy Lett. 2024, 9, 3019−3026

Table 1. $J-V$ Parameters of the NIR-TPSCs, CdTe, and 4-T CdTe/Perovskite Thin Film Tandem Solar Cells[a]

Device	Active area (aa) [cm^2]	Direction	J_{SC} [mA cm^{-2}]	V_{oc} [V]	FF [%]	PCE [%]
NIR-T PSC (n-i-p)	0.175	FS	23.68	1.06	70.2	17.62
		RS	23.75	1.07	72.0	18.30
NIR-T PSC (n-i-p)	0.805	FS	23.04	1.00	60.5	13.94
		RS	23.24	1.04	63.0	15.23
CdTe stand alone			27.38	0.87	82.1	19.56
Perovskite Filtered CdTe	-	-	8.25	0.87	82.1	5.90
4T with CdTe + 0.175 cm^2 NIR-T PSC	-	-	-	-	-	24.20
4T with CdTe + 0.805 cm^2 NIR-T PSC	-	-	-	-	-	21.13

[a]FS stands for forward scan, RS stands for reverse scan.

h, confirming their excellent operational reliability.[40−42] Figure 2c shows the steady-state power output (SPO) of the NIR-TPSC device at the maximum power point (MPP) for 300 s at a constant bias voltage of 0.80 V. The measured SPO for fabricated NIR-TPSCs is 17.4%. The above results further concluded that the fabricated devices have outstanding operational stability at constant illumination and active bias conditions.[43−46] We also performed a device stability test under continuous of 1-Sun illumination in a N_2 atmosphere (Figure S5). The device retains 80% of its initial efficiency up to ∼200 h. We have also developed inverted architecture (*p-i-n*) based triple-cation NIR-TPSCs to gain better insights into these NIR-transparent PVs and establish the operational viability of thin film tandem PVs. The small- and large-area-based devices show the highest PCE values, 17.6% and 15.0%, respectively. The details of the device's performance are listed in **Note 2** of SI.

According to the literature, theoretical study shows that the optimum bandgap (used for this study; 1.63 eV) of the perovskite absorber as a top cell with respect to 1.4 eV CdTe absorber as the bottom cell has a wider range from 1.5 to 3 eV to deliver PCE more than 30%. It is evident from these calculations that 4-T is more forgiving in terms of choice for top cell E_g of 1.4 eV CdTe as bottom cell, whereas 2-T has a drastic change. In the 4-T tandem configuration, the top subcell acts as an optical filter for the bottom subcell. In this work, we use high bandgap PSCs (E_g ∼ 1.63 eV; λ_{edge} ∼ 760 nm) as the top cell and low bandgap CdTe (E_g ∼ 1.39 eV; λ_{edge} ∼ 892 nm) as the bottom cell. Figure 3a shows the 4-T CdTe/perovskite solar cell with an index-matching liquid (silicone oil). During 4-T CdTe/perovskite tandem device measurements, an air gap is present between both cells. Optical losses owing to reflection at the top surface of the CdTe solar cell need to be addressed. An index-matched liquid helped to overcome the reflection losses from the bottom surface and couple transmitted light into the bottom cell. This work addressed the above issue. Here, we have used index-matching liquid having a refractive index (RI) of 1.405, between those of the PSCs and CdTe solar cells. Interestingly, we observed an outstanding performance boost in the PCE after adding index-matching liquid. The effect of index-matching liquid incorporation before and after, with a filtered EQE spectrum, is shown in Figure 3b. Table 2 shows the $J-V$ parameters of the filtered CdTe EQE spectrum before and after the index-matched liquid is introduced. It is observed that the transmission had improved due to index-matching liquid insertion between the subcells. This improved transmission further improved the overall current density of the bottom subcell.

Table 2. $J-V$ Parameters of the NIR-TPSCs Filtered CdTe Solar Cell Obtained from the EQE Spectrum with and without Index Matched Liquid Interlayer

Cells	J_{SC} [mA cm^{-2}]	V_{OC} [V]	FF [%]	PCE [%]
Filtered CdTe without oil (*n-i-p*)	7.15	0.87	82.1	5.12
Filtered CdTe with oil (*n-i-p*)	8.25	0.87	82.1	5.90

Figure 4a shows a schematic diagram of a 4-T CdTe/perovskite solar cell. The structure of the CdTe solar cell is glass/FTO/$Mg_{0.23}Zn_{0.77}O$/CdTe/Te/carbon paint/Ni paint/

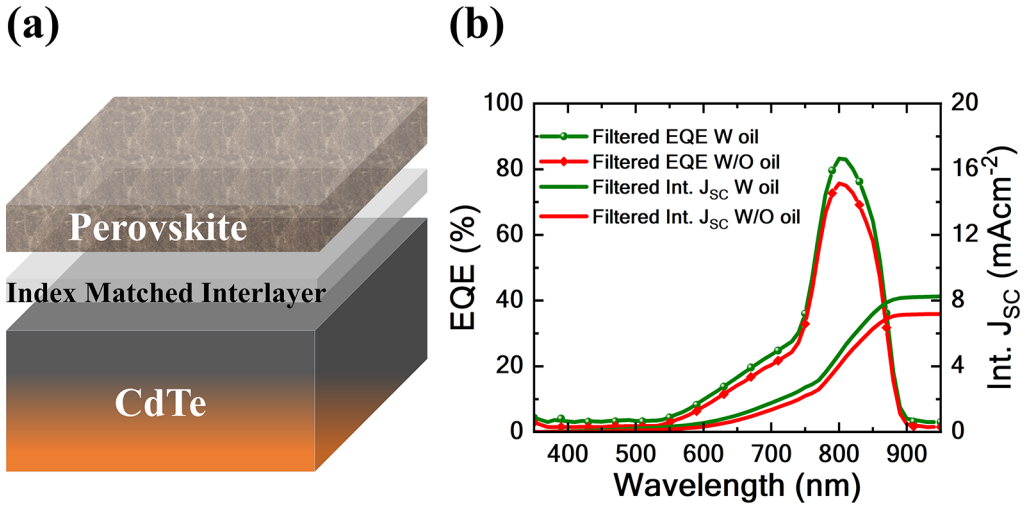

Figure 3. (a) Schematic representation of a 4-T CdTe/perovskite tandem solar cell with an index matched liquid interlayer. (b) NIR-TPSC filtered CdTe solar cell's EQE spectrum with and without an index matched liquid interlayer introduced.

https://doi.org/10.1021/acsenergylett.4c01118
ACS Energy Lett. 2024, 9, 3019−3026

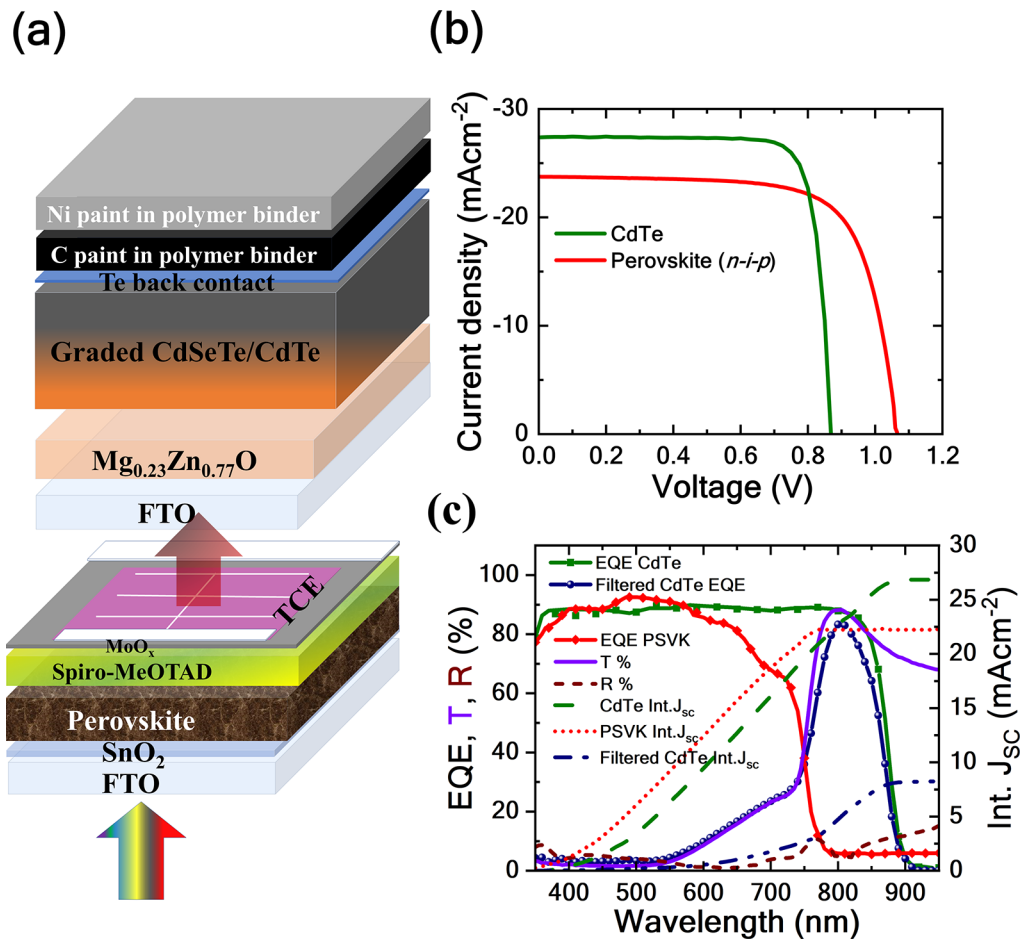

Figure 4. (a) Schematic representation of a 4-T CdTe/perovskite tandem solar cell. (b) *J*–*V* characteristics of the *n-i-p* NIR-TPSCs and CdTe solar cell. (c) EQE spectrum of *n-i-p* NIR-TPSCs and CdTe solar cell along with NIR-TPSC filtered CdTe EQE and the transmission and refraction spectra of NIR-TPSCs.

ARC. Figure 4b shows the current density–voltage (*J*–*V*) characteristics under 1-Sun illumination of the NIR-TPSCs and CdTe cells. Figure 4c shows the reflection (R%), and transmission (T%) spectra of NIR-TPSCs along with the EQE spectrum of NIR-TPSCs and CdTe cells before and after filtering through top perovskite solar cells. We observed an integrated current density (Int. *Jsc*) of 22.32 mA cm^{-2} for NIR-TPSCs-based devices. The current density deviation between J_{SC} observed from *EQE* and measured from *J*–*V* data can be attributed to a prebias measurement condition or edge effect of the device's active area.[47−49] The reduction of EQE after 600 nm is attributed to less absorption, which led to the rise of the transmission for the bottom cell. The PCE values of the unfiltered NIR-TPSC and CdTe PV devices were 18.3% and 19.56%, respectively. The perovskite filtered CdTe showed the highest PCE of 5.9%, with filtered Int. J_{SC} of 8.25 mA cm^{-2} and that led to the development of 24.2% efficient 4-T CdTe/perovskite tandem solar cells. The large-area-based devices show the highest PCE of 21.13%. The 4-T tandem cell *J*–*V* parameters before and after the filter are shown in Table 1. The efficient tandem cell configuration observed a significant PCE boost of ∼24%; 19.56% → 24.2%.

In conclusion, this study represents the first experimental demonstration of 4-T CdTe/perovskite tandem cells with a PCE exceeding 24%. We have fabricated low-temperature-processed efficient NIR-TPSCs with the highest PCE of 18.3% and average transparency T_{avg} ∼ 24.76% in the 300–900 nm wavelength range. Our fabricated NIR-TPSCs also demonstrate impressive stability, maintaining T_{80} for over 3000 h under dark storage conditions within a nitrogen (N_2) glovebox. We also demonstrated an experimental investigation of 4-T CdTe/perovskite tandem solar cells with PCEs exceeding 24%. This is accomplished by mechanical stacking wide bandgap (E_g ∼ 1.63 eV) perovskite as the top cells and low bandgap CdTe (E_g ∼ 1.39 *eV*) as the bottom cells. Additionally, the introduction of an index-matching liquid with a refractive index (RI) of 1.405 between the two subcells resulted in a PCE exceeding 24%. To the best of our knowledge, this achievement represents the highest reported PCE for a 4-T CdTe/perovskite thin-film-based tandem solar cell.

■ ASSOCIATED CONTENT

Supporting Information

The Supporting Information is available free of charge at https://pubs.acs.org/doi/10.1021/acsenergylett.4c01118.

Experimental details for the tandem solar cell fabrication, device characterization description, current density vs voltage (*J*–*V*) characteristics, SEM images, XRD pattern, EQE spectrum, and device stability. (PDF)

https://doi.org/10.1021/acsenergylett.4c01118
ACS Energy Lett. 2024, 9, 3019−3026

AUTHOR INFORMATION

Corresponding Author

Dinesh Kabra − *Department of Physics, Indian Institute of Technology Bombay, Powai, Mumbai 400076, India;* orcid.org/0000-0001-5256-1465; Email: dkabra@iitb.ac.in

Authors

Ananta Paul − *Department of Metallurgical Engineering and Material Science, Indian Institute of Technology Bombay, Mumbai 400076, India*

Abhijit Singha − *Department of Energy Science and Engineering, Indian Institute of Technology Bombay, Mumbai 400076, India*

Kashimul Hossain − *Department of Physics, Indian Institute of Technology Bombay, Powai, Mumbai 400076, India*

Saurabh Gupta − *Department of Physics, Indian Institute of Technology Bombay, Powai, Mumbai 400076, India*

Manas Misra − *Department of Physics, Indian Institute of Technology Bombay, Powai, Mumbai 400076, India*

Sudhanshu Mallick − *Department of Metallurgical Engineering and Material Science, Indian Institute of Technology Bombay, Mumbai 400076, India;* orcid.org/0000-0002-9744-8746

Amit H. Munshi − *Department of Mechanical Engineering, Colorado State University, Fort Collins, Colorado 80523, United States;* orcid.org/0000-0002-9949-9600

Complete contact information is available at: https://pubs.acs.org/10.1021/acsenergylett.4c01118

Author Contributions

†A.P., A.S., and K.H. contributed equally to this work.

Notes

This report has been prepared as a documentation of work supported by a United States Government agency. The United States Government, its agencies, and their employees do not provide any warranty, express or implied, and assume no legal liability or responsibility for the accuracy, completeness, or usefulness of the disclosed information, apparatus, product, or process. Additionally, it is not implied that the use of such information would not infringe privately owned rights. Mention of specific commercial products, processes, or services by trade name, trademark, manufacturer, or otherwise, does not necessarily imply endorsement, recommendation, or favoring by the United States Government or any of its agencies. The views and opinions expressed in this report by the authors do not necessarily represent those of the United States Government or any of its agencies.

The authors declare no competing financial interest.

ACKNOWLEDGMENTS

The authors acknowledge MoE-India for the doctoral fellowship. This work was also partially supported by a DST-Solar Challenge Award (DST/ETC/CASE/RES/2023/02). D.K. also acknowledges Forbes Marshall financial support for the Energy Science and Engineering chair professorship. The authors also acknowledge the micro factory lab for fabricating the mask. The authors are also thankful to Rory Back and Su Verma from NSG Pilkington for providing the FTO substrates. Colorado State University expresses gratitude for the valuable in-kind semiconductor material support provided by 5N Plus Inc., which was utilized in the fabrication of high-efficiency CdTe PV devices. The utilization of this material is attributed in part to the support received from the U.S. Department of Energy's Office of Science under Award Number DE-SC0022812. Furthermore, the development of this journal article received partial funding from the Alliance for Sustainable Energy, LLC, the Managing and Operating Contractor for the National Renewable Energy Laboratory for the U.S. Department of Energy. The authors also extend their appreciation for the support received from the National Science Foundation under the Industry/University Cooperative Research Center (I/UCRC) for the Next Generation Photovoltaics program (Award Number −1821526), as well as the I/UCRC for Next Generation Photovoltaics Industrial Advisory Board.

REFERENCES

(1) Goldemberg, J.; United Nations Development Programme.; United Nations. Department of Economic and Social Affairs; World Energy Council; *World Energy Assessment : Energy and the Challenge of Sustainability*; United Nations Development Programme, 2000.

(2) Scarpulla, M. A.; McCandless, B.; Phillips, A. B.; Yan, Y.; Heben, M. J.; Wolden, C.; Xiong, G.; Metzger, W. K.; Mao, D.; Krasikov, D.; Sankin, I.; Grover, S.; Munshi, A.; Sampath, W.; Sites, J. R.; Bothwell, A.; Albin, D.; Reese, M. O.; Romeo, A.; Nardone, M.; Klie, R.; Walls, J. M.; Fiducia, T.; Abbas, A.; Hayes, S. M. CdTe-Based Thin Film Photovoltaics: Recent Advances, Current Challenges and Future Prospects. *Sol. Energy Mater. Sol. Cells* **2023**, *255*, No. 112289.

(3) Singha, A.; Paul, A.; Koul, S.; Sharma, V.; Mallick, S.; Balasubramaniam, K. R.; Kabra, D. Stable and Efficient Large-Area 4T Si/Perovskite Tandem Photovoltaics with Sputtered Transparent Contact. *Solar RRL* **2023**, *7* (12), No. 2300117.

(4) Hossain, K.; Kulkarni, A.; Bothra, U.; Klingebiel, B.; Kirchartz, T.; Saliba, M.; Kabra, D. Resolving the Hydrophobicity of Me-4PACz Hole Transport Layer for High-Efficiency Inverted Perovskite Solar Cells. *ACS Energy Lett.* **2023**, *8* (9), 3860−3867.

(5) Zhou, J.; Tan, L.; Liu, Y.; Li, H.; Liu, X.; Li, M.; Wang, S.; Zhang, Y.; Jiang, C.; Hua, R.; Tress, W.; Meloni, S.; Yi, C. Highly Efficient and Stable Perovskite Solar Cells via a Multifunctional Hole Transporting Material. *Joule* **2024**, *8*, 1−16.

(6) Hossain, K.; Sivadas, D.; Kabra, D.; Nair, P. R. Perovskite Solar Cells Dominated by Bimolecular Recombination—How Far Is the Radiative Limit? *ACS Energy Lett.* **2024**, *9*, 2310−2317.

(7) Prasanna, R.; Gold-Parker, A.; Leijtens, T.; Conings, B.; Babayigit, A.; Boyen, H. G.; Toney, M. F.; McGehee, M. D. Band Gap Tuning via Lattice Contraction and Octahedral Tilting in Perovskite Materials for Photovoltaics. *J. Am. Chem. Soc.* **2017**, *139* (32), 11117−11124.

(8) Sharma, R.; Jain, N.; Lee, H.; Kabra, D.; Yoo, S. Comprehensive and Comparative Analysis of Photoinduced Charge Generation, Recombination Kinetics, and Energy Losses in Fullerene and Nonfullerene Acceptor-Based Organic Solar Cells. *ACS Appl. Mater. Interfaces* **2020**, *12* (40), 45083−45091.

(9) Guchhait, A.; Dewi, H. A.; Leow, S. W.; Wang, H.; Han, G.; Suhaimi, F. B.; Mhaisalkar, S.; Wong, L. H.; Mathews, N. Over 20% Efficient CIGS-Perovskite Tandem Solar Cells. *ACS Energy Lett.* **2017**, *2* (4), 807−812.

(10) Jošt, M.; Köhnen, E.; Al-Ashouri, A.; Bertram, T.; Tomšič, Š.; Magomedov, A.; Kasparavicius, E.; Kodalle, T.; Lipovšek, B.; Getautis, V.; Schlatmann, R.; Kaufmann, C. A.; Albrecht, S.; Topič, M. Perovskite/CIGS Tandem Solar Cells: From Certified 24.2% toward 30% and Beyond. *ACS Energy Lett.* **2022**, *7* (4), 1298−1307.

(11) Kumar, A.; Singh, S.; Mohammed, M. K. A.; Shalan, A. E. Computational Modelling of Two Terminal CIGS/Perovskite Tandem Solar Cells with Power Conversion Efficiency of 23.1%. *Eur. J. Inorg. Chem.* **2021**, *2021* (47), 4959−4969.

(12) Jiang, Y.; Feurer, T.; Carron, R.; Sevilla, G. T.; Moser, T.; Pisoni, S.; Erni, R.; Rossell, M. D.; Ochoa, M.; Hertwig, R.; Tiwari, A.

N.; Fu, F. High-Mobility In2O3:H Electrodes for Four-Terminal Perovskite/CuInSe2Tandem Solar Cells. *ACS Nano* **2020**, *14* (6), 7502−7512.
(13) Ruiz-Preciado, M. A.; Gota, F.; Fassl, P.; Hossain, I. M.; Singh, R.; Laufer, F.; Schackmar, F.; Feeney, T.; Farag, A.; Allegro, I.; Hu, H.; Gharibzadeh, S.; Nejand, B. A.; Gevaerts, V. S.; Simor, M.; Bolt, P. J.; Paetzold, U. W. Monolithic Two-Terminal Perovskite/CIS Tandem Solar Cells with Efficiency Approaching 25%. *ACS Energy Lett.* **2022**, *7* (7), 2273−2281.
(14) He, R.; Ren, S.; Chen, C.; Yi, Z.; Luo, Y.; Lai, H.; Wang, W.; Zeng, G.; Hao, X.; Wang, Y.; Zhang, J.; Wang, C.; Wu, L.; Fu, F.; Zhao, D. Wide-Bandgap Organic-Inorganic Hybrid and All-Inorganic Perovskite Solar Cells and Their Application in All-Perovskite Tandem Solar Cells. *Energy Environ. Sci.* **2021**, *14* (11), 5723−5759.
(15) Lal, N. N.; Dkhissi, Y.; Li, W.; Hou, Q.; Cheng, Y. B.; Bach, U. Perovskite Tandem Solar Cells. *Adv. Energy Mater.* **2017**, *7* (18), No. 1602761.
(16) Brinkmann, K. O.; Becker, T.; Zimmermann, F.; Kreusel, C.; Gahlmann, T.; Theisen, M.; Haeger, T.; Olthof, S.; Tückmantel, C.; Günster, M.; Maschwitz, T.; Göbelsmann, F.; Koch, C.; Hertel, D.; Caprioglio, P.; Peña-Camargo, F.; Perdigón-Toro, L.; Al-Ashouri, A.; Merten, L.; Hinderhofer, A.; Gomell, L.; Zhang, S.; Schreiber, F.; Albrecht, S.; Meerholz, K.; Neher, D.; Stolterfoht, M.; Riedl, T. Perovskite−Organic Tandem Solar Cells with Indium Oxide Interconnect. *Nature* **2022**, *604* (7905), 280−286.
(17) Akhil, S.; Akash, S.; Pasha, A.; Kulkarni, B.; Jalalah, M.; Alsaiari, M.; Harraz, F. A.; Balakrishna, R. G. Review on Perovskite Silicon Tandem Solar Cells: Status and Prospects 2T, 3T and 4T for Real World Conditions. *Mater. Des* **2021**, *211*, No. 110138.
(18) Li, T. T.; Yang, Y. B.; Li, G. R.; Chen, P.; Gao, X. P. Two-Terminal Perovskite-Based Tandem Solar Cells for Energy Conversion and Storage. *Small* **2021**, *17* (23), No. 2006145.
(19) Kamide, K.; Takato, H. A Current Matching Design and Its Impact of High-Efficiency Two-Terminal Perovskite/Silicon Tandem Photovoltaics. *IEEE J. Photovolt* **2023**, *13* (5), 699−704.
(20) Kim, D. H.; Muzzillo, C. P.; Tong, J.; Palmstrom, A. F.; Larson, B. W.; Choi, C.; Harvey, S. P.; Glynn, S.; Whitaker, J. B.; Zhang, F.; Li, Z.; Lu, H.; van Hest, M. F. A. M.; Berry, J. J.; Mansfield, L. M.; Huang, Y.; Yan, Y.; Zhu, K. Bimolecular Additives Improve Wide-Band-Gap Perovskites for Efficient Tandem Solar Cells with CIGS. *Joule* **2019**, *3* (7), 1734−1745.
(21) Wang, W.; Liu, X.; Wang, J.; Chen, C.; Yu, J.; Zhao, D.; Tang, W. Versatile Self-Assembled Molecule Enables High-Efficiency Wide-Bandgap Perovskite Solar Cells and Organic Solar Cells. *Adv. Energy Mater.* **2023**, *13* (23), No. 2300694.
(22) Liu, L.; Xiao, H.; Jin, K.; Xiao, Z.; Du, X.; Yan, K.; Hao, F.; Bao, Q.; Yi, C.; Liu, F.; Wang, W.; Zuo, C.; Ding, L. 4-Terminal Inorganic Perovskite/Organic Tandem Solar Cells Offer 22% Efficiency. *Nanomicro Lett.* **2023**, *15* (1), 23.
(23) Wang, P.; Wu, Y.; Cai, B.; Ma, Q.; Zheng, X.; Zhang, W. H. Solution-Processable Perovskite Solar Cells toward Commercialization: Progress and Challenges. *Adv. Funct Mater.* **2019**, *29* (47), No. 1807661.
(24) Romeo, N.; Bosio, A.; Menossi, D.; Romeo, A.; Aramini, M. Last Progress in CdTe/CdS Thin Film Solar Cell Fabrication Process. *Energy Procedia*; Elsevier Ltd, 2014; Vol. *57*, pp 65−72. DOI: 10.1016/j.egypro.2014.10.009.
(25) Sofia, S. E.; Mailoa, J. P.; Weiss, D. N.; Stanbery, B. J.; Buonassisi, T.; Peters, I. M. Economic Viability of Thin-Film Tandem Solar Modules in the United States /639/4077/909/4101/4096 /706/4066/4068 Article. *Nat. Energy* **2018**, *3* (5), 387−394.
(26) Razykov, T. M.; Ferekides, C. S.; Morel, D.; Stefanakos, E.; Ullal, H. S.; Upadhyaya, H. M. Solar Photovoltaic Electricity: Current Status and Future Prospects. *Sol. Energy* **2011**, *85* (8), 1580−1608.
(27) Song, Z.; Subedi, K. K.; Ellingson, R.; Yan, Y. Architecture for Efficient Monolithic Bifacial Perovskite-CdSeTe Tandem Thin Solar Cells and Modules. US 2022/0199845 A1, June 20202.
(28) Hu, Z.; An, Q.; Xiang, H.; Aigouy, L.; Sun, B.; Vaynzof, Y.; Chen, Z. Enhancing the Efficiency and Stability of Triple-Cation Perovskite Solar Cells by Eliminating Excess PbI2from the Perovskite/Hole Transport Layer Interface. *ACS Appl. Mater. Interfaces* **2020**, *12* (49), 54824−54832.
(29) Kress, J. A.; Quarti, C.; An, Q.; Bitton, S.; Tessler, N.; Beljonne, D.; Vaynzof, Y. Persistent Ion Accumulation at Interfaces Improves the Performance of Perovskite Solar Cells. *ACS Energy Lett.* **2022**, *7* (10), 3302−3310.
(30) Chee, A. K. W. On Current Technology for Light Absorber Materials Used in Highly Efficient Industrial Solar Cells. *Renewable and Sustainable Energy Reviews* **2023**, *173*, No. 113027.
(31) Yang, Q.; Duan, W.; Eberst, A.; Klingebiel, B.; Wang, Y.; Kulkarni, A.; Lambertz, A.; Bittkau, K.; Zhang, Y.; Vitusevich, S.; Rau, U.; Kirchartz, T.; Ding, K. Origin of Sputter Damage during Transparent Conductive Oxide Deposition for Semitransparent Perovskite Solar Cells. *J. Mater. Chem. A Mater.* **2024**, DOI: 10.1039/D3TA06654A.
(32) Bett, A. J.; Winkler, K. M.; Bivour, M.; Cojocaru, L.; Kabakli, Ö.; Schulze, P. S. C.; Siefer, G.; Tutsch, L.; Hermle, M.; Glunz, S. W.; Goldschmidt, J. C. Semi-Transparent Perovskite Solar Cells with ITO Directly Sputtered on Spiro-OMeTAD for Tandem Applications. *ACS Appl. Mater. Interfaces* **2019**, *11* (49), 45796−45804.
(33) Sharma, B.; Singh, S.; Hossain, K.; Laxmi; Mallick, S.; Bhargava, P.; Kabra, D. Additive Engineering of 4, 4′-Bis (N-Carbazolyl)-1, 1′-Biphenyl (CBP) Molecules for Defects Passivation and Moisture Stability of Hybrid Perovskite Layer. *Sol. Energy* **2020**, *211*, 1084−1091.
(34) Aranda, C. A.; Alvarez, A. O.; Chivrony, V. S.; Das, C.; Rai, M.; Saliba, M. Overcoming Ionic Migration in Perovskite Solar Cells through Alkali Metals. *Joule* **2024**, *8* (1), 241−254.
(35) Yuan, Q.; Lohmann, K. B.; Oliver, R. D. J.; Ramadan, A. J.; Yan, S.; Ball, J. M.; Christoforo, M. G.; Noel, N. K.; Snaith, H. J.; Herz, L. M.; Johnston, M. B. Thermally Stable Perovskite Solar Cells by All-Vacuum Deposition. *ACS Appl. Mater. Interfaces* **2023**, *15* (1), 772−781.
(36) Rehman, A. ur; Van Kerschaver, E. P.; Aydin, E.; Raja, W.; Allen, T. G.; De Wolf, S. Electrode Metallization for Scaled Perovskite/Silicon Tandem Solar Cells: Challenges and Opportunities. *Progress in Photovoltaics: Research and Applications* **2023**, *31* (4), 429−442.
(37) Werner, J.; Barraud, L.; Walter, A.; Bräuninger, M.; Sahli, F.; Sacchetto, D.; Tétreault, N.; Paviet-Salomon, B.; Moon, S. J.; Allebé, C.; Despeisse, M.; Nicolay, S.; De Wolf, S.; Niesen, B.; Ballif, C. Efficient Near-Infrared-Transparent Perovskite Solar Cells Enabling Direct Comparison of 4-Terminal and Monolithic Perovskite/Silicon Tandem Cells. *ACS Energy Lett.* **2016**, *1* (2), 474−480.
(38) Yang, D.; Zhou, X.; Yang, R.; Yang, Z.; Yu, W.; Wang, X.; Li, C.; Liu, S.; Chang, R. P. H. Surface Optimization to Eliminate Hysteresis for Record Efficiency Planar Perovskite Solar Cells. *Energy Environ. Sci.* **2016**, *9* (10), 3071−3078.
(39) Yang, D.; Yang, R.; Wang, K.; Wu, C.; Zhu, X.; Feng, J.; Ren, X.; Fang, G.; Priya, S.; Liu, S. F. High Efficiency Planar-Type Perovskite Solar Cells with Negligible Hysteresis Using EDTA-Complexed SnO2. *Nat. Commun.* **2018**, *9* (1), 3239.
(40) Yang, H.; Shen, Y.; Zhang, R.; Wu, Y.; Chen, W.; Yang, F.; Cheng, Q.; Chen, H.; Ou, X.; Yang, H.; Gao, F.; Li, Y.; Li, Y. Composition-Conditioning Agent for Doped Spiro-OMeTAD to Realize Highly Efficient and Stable Perovskite Solar Cells. *Adv. Energy Mater.* **2022**, *12* (44), No. 2202207.
(41) Zhang, T.; Wang, F.; Kim, H.-B.; Choi, I.-W.; Wang, C.; Cho, E.; Konefal, R.; Puttisong, Y.; Terado, K.; Kobera, L.; Chen, M.; Yang, M.; Bai, S.; Yang, B.; Suo, J.; Yang, S.-C.; Liu, X.; Fu, F.; Yoshida, H.; Chen, W. M.; Brus, J.; Coropceanu, V.; Hagfeldt, A.; Brédas, J.-L.; Fahlman, M.; Suk Kim, D.; Hu, Z.; Gao, F. Ion-Modulated Radical Doping of Spiro-OMeTAD for More Efficient and Stable Perovskite Solar Cells. *Science (1979)* **2022**, *377*, 495−501.
(42) Zhao, X.; Liu, T.; Burlingame, Q. C.; Liu, T.; Holleyiii, R.; Cheng, G.; Yao, N.; Gao, F.; Loo, Y.-L. Accelerated Aging of All-Inorganic, Interface-Stabilized Perovskite Solar Cells. *Science (1979)* **2022**, *377* (6603), 307−310.

(43) Ye, Y. C.; Chen, L.; Chen, X. M.; Ma, C. Y.; Lv, B. H.; Wang, J. Y.; Dou, W. D.; Zhang, C.; Ma, T. L.; Tang, J. X. Interfacial Energy Level Alignment and Defect Passivation by Using a Multifunctional Molecular for Efficient and Stable Perovskite Solar Cells. *Adv. Funct Mater.* **2024**, *34* (8), No. 2310136.
(44) Jiang, Q.; Song, Z.; Bramante, R. C.; Ndione, P. F.; Tirawat, R.; Berry, J. J.; Yan, Y.; Zhu, K. Highly Efficient Bifacial Single-Junction Perovskite Solar Cells. *Joule* **2023**, *7* (7), 1543−1555.
(45) Habisreutinger, S. N.; Wenger, B.; Snaith, H. J.; Nicholas, R. J. Dopant-Free Planar n-i-p Perovskite Solar Cells with Steady-State Efficiencies Exceeding 18%. *ACS Energy Lett.* **2017**, *2* (3), 622−628.
(46) Habisreutinger, S. N.; Noel, N. K.; Snaith, H. J.; Nicholas, R. J. Investigating the Role of 4-Tert Butylpyridine in Perovskite Solar Cells. *Adv. Energy Mater.* **2017**, *7* (1), No. 1601079.
(47) Hossain, K.; Singh, S.; Kabra, D. Role of Monovalent Cations in the Dielectric Relaxation Processes in Hybrid Metal Halide Perovskite Solar Cells. *ACS Appl. Energy Mater.* **2022**, *5* (3), 3689−3697.
(48) Ravishankar, S.; Aranda, C.; Boix, P. P.; Anta, J. A.; Bisquert, J.; Garcia-Belmonte, G. Effects of Frequency Dependence of the External Quantum Efficiency of Perovskite Solar Cells. *J. Phys. Chem. Lett.* **2018**, *9* (11), 3099−3104.
(49) Saliba, M.; Etgar, L. Current Density Mismatch in Perovskite Solar Cells. *ACS Energy Lett.* **2020**, *5* (9), 2886−2888.

https://doi.org/10.1021/acsenergylett.4c01118
ACS Energy Lett. 2024, 9, 3019−3026